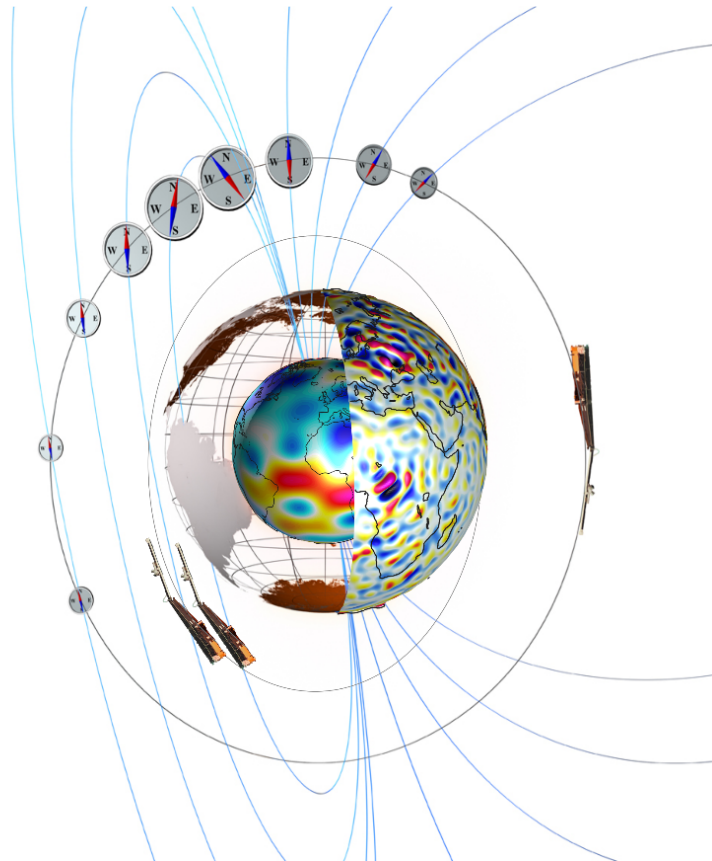




# Swarm-IPIR Description of the Processing Algorithm



Doc. no: SW-TN-UiO-GS-003, Rev: 1B, 08 Sept. 2019

Prepared:

Prepared:

Yaqi Jin

Date 08 Sept. 2019

Chao Xiong

Date 02 Nov. 2019

Scientist

Scientist

Approved:

Wojciech J. Miloch

Date 08 Sept. 2019

Project Manager

© UiO, Norway, 2019, GFZ, Germany 2018. Proprietary and intellectual rights of UiO, Norway and GFZ, Germany, are involved in the subject-matter of this material and all manufacturing, reproduction, use, disclosure, and sales rights pertaining to such subject-matter are expressly reserved. This material is submitted for a specific purpose as agreed in writing, and the recipient by accepting this material agrees that this material will not be used, copied, or reproduced in whole or in part nor its contents (or any part thereof) revealed in any manner or to any third party, except own staff, to meet the purpose for which it was submitted and subject to the terms of the written agreement.



## Record of Changes

Reason	Description	Rev	Date
Initial vers.	Released	1 dA	05 May 2018
Revised IPIR index and minor corrections.	Released	2 dA	28 Aug 2018
Final version	Corrected entries, version number, formatting, and parts of text	1A	01 Sept 2018
Final version	Updated section 5: Description of the output data	1B	02 Nov 2018
Final version	Removed table 1 in section 5, as the full list of parameters is found in the Product Definition Document.	1C	08 Sept 2019



## Table of Contents

<b>1</b>	<b>Introduction .....</b>	<b>7</b>
1.1	Scope and applicability.....	7
<b>2</b>	<b>Applicable and Reference Documentation.....</b>	<b>7</b>
2.1	Applicable Documents .....	7
2.2	Reference Documents.....	7
2.3	Abbreviations .....	8
<b>3</b>	<b>Scientific Background .....</b>	<b>10</b>
<b>4</b>	<b>Algorithms Description.....</b>	<b>11</b>
4.1	Processing algorithm – block diagram .....	11
4.2	Algorithms for irregularity parameters from Swarm satellites .....	11
4.2.1	Characteristics of electron density fluctuations.....	11
4.2.2	Mathematical description of electron density parameters.....	11
4.2.3	ROT and ROTI from the GPS TEC data .....	14
4.3	Assigning plasma irregularities to geomagnetic regions.....	15
4.3.1	Auroral oval boundaries: the FAC method .....	15
4.3.1.1	Module 1: read configuration file.....	16
4.3.1.2	Module 2: data pre-processing .....	17
4.3.1.3	Module 3: finding the auroral equatorial boundary.....	17
4.3.1.4	Module 4: finding the auroral poleward boundary.....	17
4.3.1.5	Module 5: saving of Swarm AOB data .....	17
4.4	Determining the IPIR-index .....	17
<b>5</b>	<b>Description of the output data .....</b>	<b>19</b>
<b>6</b>	<b>Selected Examples .....</b>	<b>20</b>



## 1 Introduction

### 1.1 Scope and applicability

This document comprises the Swarm Level 2 (L2) IPIR product Description of the Processing Algorithm (DPA) document for the Swarm Data, Innovation and Science Cluster (Swarm DISC) consortium in response to the requirements of [AD-1]. Swarm-IPIR uses the following products [AD-4]:

- EFix\_PL\_1B – 2Hz data from the Electrical Field Instrument (EFI).
- TECxTMS\_2F – TEC data derived from onboard GPS.
- AOBxFAC\_2F – Auroral Oval Boundaries (AOB) using the Field-Aligned Current (FAC) method.
- IBIXTMS\_2F, IBI: Ionospheric Bubble Index.
- Polar Cap Products (PCP).

The Swarm-IPIR Product Definition document [AD-4] is available in the SVN folder: [https://smart-svn.spacecenter.dk/svn/smart/SwarmDISC/DISC\\_Projects/ITT1\\_4\\_ionospheric\\_irregularities/Deliverables/](https://smart-svn.spacecenter.dk/svn/smart/SwarmDISC/DISC_Projects/ITT1_4_ionospheric_irregularities/Deliverables/).

Current or updated version of this document is available in the SVN folder: [https://smart-svn.spacecenter.dk/svn/smart/SwarmDISC/DISC\\_Projects/ITT1\\_4\\_ionospheric\\_irregularities/Deliverables/](https://smart-svn.spacecenter.dk/svn/smart/SwarmDISC/DISC_Projects/ITT1_4_ionospheric_irregularities/Deliverables/).

## 2 Applicable and Reference Documentation

### 2.1 Applicable Documents

The following documents are applicable to the definitions within this document.

- [AD-1] SW-SW-DTU-GS-114, rev 1 Statement of Work for Swarm DISC ITT 1.4 “Ionospheric irregularities and fluctuations based on Swarm data”
- [AD-2] IPIR-Swarm-IPIR-12017 – Ionospheric Plasma Irregularities characterised by the Swarm satellites.
- [AD-3] <https://earth.esa.int/web/guest/missions/esa-eo-missions/swarm/data-handbook>
- [AD-4] SW-TN-UIO-GS-001, Swarm-IPIR Product Definition.

### 2.2 Reference Documents

The following documents contain supporting and background information to be taken into account during the activities specified within this document.

- [RD-1] Feldstein Y. I. et al. (1969) Phenomenology and morphology of aurorae, Ann. Int. Quiet Sun Year, 4, 311-348.
- [RD-2] Kauristie, K., et al. (1999) Size of the auroral oval: UV ovals and precipitation boundaries compared, J. Geophys. Res., 104, 2321–2331
- [RD-3] Kelley, M. C. (2009), The Earth’s Ionosphere Plasma Physics and Electrodynamics Second Edition, Elsevier, Amsterdam.
- [RD-4] Kintner, P. M., B. M. Ledvina, and E. R. de Paula (2007), GPS and ionospheric scintillations, Space Weather, 5, S09003.

- [RD-5] Lorentzen, D.A. (2000), Latitudinal and longitudinal dispersion of energetic auroral protons, *Ann. Geophys.*, 18, 81.
- [RD-6] Newell, P. T., C.-I. Meng, D. G. Sibeck, and R. Lepping (1989), Some low-altitude cusp dependencies on the interplanetary magnetic field, *J. Geophys. Res.*, 94, 8921–8927.
- [RD-7] Moen et al., (2004) The dynamics and relationships of precipitation, temperature and convection boundaries in the dayside auroral ionosphere, *Ann. Geophys.*, 22, 1973–1987.
- [RD-8] Pinnock, M. and Rodger, A. S. (2000), On determining the noon polar cap boundary from Super-DRN HF radar backscatter characteristics, *Ann. Geophys.*, 18, 1523–1530
- [RD-9] Park, J., Lühr, H., Min, K. (2010): Neutral density depletions associated with equatorial plasma bubbles as observed by the CHAMP satellite, *Journal of Atmospheric and Solar-Terrestrial Physics*, 72, 2-3, p. 157-163.
- [RD-10] Richmond, A. D. (1995), Ionospheric electrodynamics using magnetic apex coordinates, *J. Geomagn. Geoelectr.*, 47, 191–212
- [RD-11] Spicher, A., et al. (2017), Interhemispheric study of polar cap patch occurrence based on Swarm in situ data, *J. Geophys. Res.*, 122, 3837–3851.
- [RD-12] Wang, H., et al (2005), Statistical study of the subauroral polarization stream: Its dependence on the cross-polar cap potential and subauroral conductance, *J. Geophys. Res.*, 113, A12311,
- [RD-13] Xiong C. and Luhr. H. (2014), An empirical model of the auroral oval derived from CHAMP field-aligned current signatures - Part 2, *Ann. Geophys.* 32, 623-632.
- [RD-14] Xiong, C., et al. (2014) Determining the boundaries of the auroral oval from CHAMP field-aligned current signatures – Part 1, *Ann. Geophys.*, 32, 609–622.
- [RD-15] Yeh, K. C., and C.H. Liu (1982), Radio wave scintillations in the ionosphere, *Proc. IEEE*, 704, 325–378. Wang et al, 2005

## 2.3 Abbreviations

<b>Acronym</b> <i>or abbreviation</i>	<b>Description</b>
AOB	Auroral Oval Boundaries
DISC	The Data, Innovation and Science Cluster
DPA	Description of the Processing Algorithm
ESA	European Space Agency
FAC	Field-Aligned Current
GFZ	The Helmholtz Centre Potsdam - GFZ German Research Centre for Geosciences, DE
L1b	Level 1b (satellite data)
L2	Level 2 (satellite data)
MLAT	Magnetic Latitude



SVN	SVN Repository with server located at DTU. Presently, the following URLs apply: <a href="https://smart-svn.spacecenter.dk/svn/smart/SwarmDISC/DISC_Projects/ITT1_4_ionospheric_irregularities/Deliverables/">https://smart-svn.spacecenter.dk/svn/smart/SwarmDISC/DISC_Projects/ITT1_4_ionospheric_irregularities/Deliverables/</a>
Swarm	Constellation of 3 ESA satellites, <a href="https://earth.esa.int/web/guest/missions/esa-operational-eo-missions/swarm">https://earth.esa.int/web/guest/missions/esa-operational-eo-missions/swarm</a>
TBD	To Be Defined
UiO	The University of Oslo, Oslo, Norway

### 3 Scientific Background

Ionospheric plasma is often characterised by irregularities and fluctuations in its density. They are the result of various plasma instabilities, which reflect complex interactions in the near-Earth space environment (Kelley 2009). Plasma density irregularities and fluctuations can influence the propagation of trans-ionospheric radio waves and are thus of importance for ground-based operations that rely on precise positioning with Global Navigation Satellite Systems (GNSS) (Yeh and Liu 1982, Kintner et al. 2007). Understanding ionospheric plasma irregularities and fluctuations is thus of both scientific and practical interest. In this document we present an algorithm for a global product based on Swarm measurements that characterizes ionospheric irregularities and fluctuations, and which addresses the needs of scientific community and operational users.

In-situ measurements of plasma irregularities and fluctuations can be successfully carried out by the Swarm satellites with their complementary datasets, i.e. the electron density from the electric field instrument, the Global Positioning System (GPS) data from the onboard GPS receiver, and the magnetic data from the vector field magnetometer, as well as Level-2 Swarm data products. In the IPIR - Ionospheric Plasma Irregularities product, we derive new parameters in addition to the existing datasets and provide comprehensive information on plasma irregularities and fluctuations at all latitudes. IPIR provides characteristics of plasma density structures in the ionosphere. It addresses the needs of scientific community, that aims to understand ionospheric plasma irregularities, as well as operational users that are affected by them.

The algorithm detects and characterises plasma irregularities along the whole satellite track, thus including also equatorial plasma bubbles and polar cap patches, which are often associated with plasma irregularities. IPIR provides characteristics of plasma irregularities in terms of their amplitudes, gradients and spatial scales and assigns them to geomagnetic regions and consequently to predominant plasma processes. It also provides indication, in the form of a numerical value index, on their severity for the integrity of trans-ionospheric radio signals and hence the accuracy of GNSS precise positioning. In order to provide this comprehensive information, the product combines Level 1b data products for Swarm: plasma density, magnetic field, and level 1 and level 2 data from the on-board GPS receivers.

The IPIR product characterises the plasma density fluctuations and irregularities encountered by Swarm in terms of their spatial occurrence and amplitudes. This can be analysed relative to the local plasma conditions, i.e., to the local background. IPIR also relates the fluctuations to the ionospheric current system and variations in the magnetic field, in order to relate these structures to dynamic phenomena in the ionosphere. Finally, it combines data from the GPS receivers, where Total Electron Content (TEC) and Rate of Change of TEC (ROT) provide information on the extent of the structures in the direction towards GPS satellites.

The operational-user oriented part of the product, the IPIR-index, combines results from different datasets and provides numeric values that will indicate the strength and scales of irregularities and the reliability of the GNSS precise positioning. It is validated against ground-based measurements, focusing on GPS TEC and scintillation data at different latitudes.

## 4 Algorithms Description

### 4.1 Processing algorithm – block diagram

The processing algorithm is summarised in Figure 4.1.1, and described in detail in the following subsections.

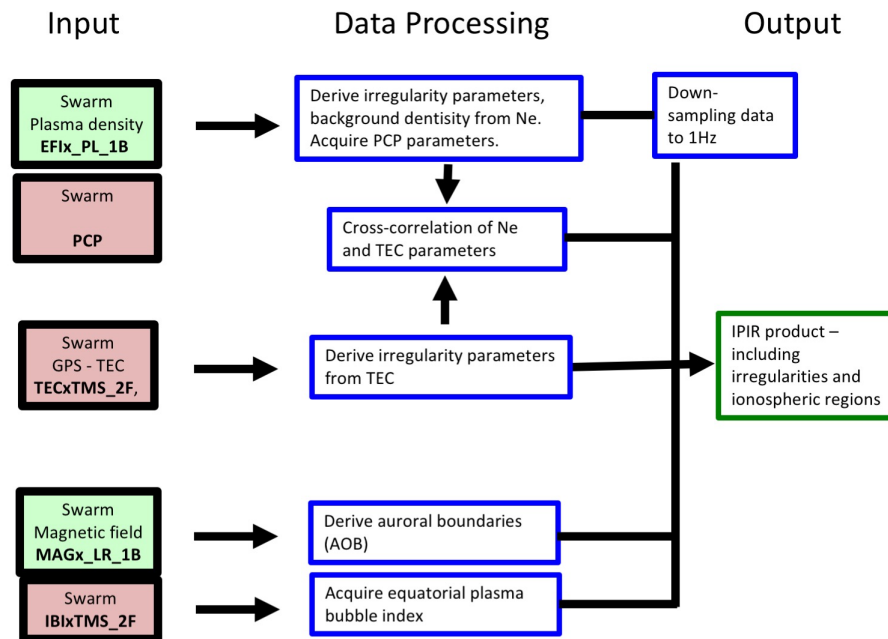


Figure 4.1.1 The overview of the IPIR processing algorithm.

## 4.2 Algorithms for irregularity parameters from Swarm satellites

### 4.2.1 Characteristics of electron density fluctuations

The electron density ( $Ne$ ) and electron temperature ( $Te$ ) data are taken from L1b dataset: EFix\_PL\_1B. From  $Ne$  data, we derive parameters that characterize the in-situ electron density fluctuations. These parameters include

- Rate of change of Density (ROD),
- Rate of change of Density Index in 10 seconds (RODI10s),
- Rate of change of Density Index in 20 seconds (RODI20s),
- filtered  $Ne$  fluctuations in 10 seconds (Delta\_Ne10s),
- filtered  $Ne$  fluctuations in 20 seconds (Delta\_Ne20s),
- filtered  $Ne$  fluctuations in 40 seconds (Delta\_Ne40s),
- $Ne$  gradient in 100 km scale (Grad\_Ne@100km),
- $Ne$  gradient in 50 km scale (Grad\_Ne@50km),
- $Ne$  gradient in 20 km scale (Grad\_Ne@20km),
- $Ne$  gradient near the edge of a polar cap patch (Grad\_Ne@PCP\_edge).

### 4.2.2 Mathematical description of electron density parameters

ROD is defined as a time derivative of the electron density:

$$ROD(t) = \frac{Ne(t + \Delta t) - Ne(t)}{\Delta t}$$

Since we use 2Hz Swarm data for accounting for small scale fluctuations,  $\Delta t = 0.5 \text{ seconds}$ .

RODI10s (RODI20s) is the standard deviation of ROD in a running window of 10 (20) seconds:

$$RODI(t) = \sqrt{\frac{1}{N-1} \sum_{t_i=t-\Delta t/2}^{t_i=t+\Delta t/2} |ROD(t_i) - \overline{ROD}|^2}$$

where  $\overline{ROD}$  is the mean of  $ROD(t_i)$ :

$$\overline{ROD} = \frac{1}{N} \sum_{t_i=t-\Delta t/2}^{t_i=t+\Delta t/2} ROD(t_i)$$

In deriving RODI10s and RODI20s, we use respectively  $\Delta t = 10$  and  $20 \text{ seconds}$ .

Filtered electron density parameters, delta\_Ne10s, delta\_Ne20s, delta\_Ne40s, are derived by subtracting the median filtered value in 10 (20, 40) seconds from  $Ne$ . Therefore, delta\_Ne10s (delta\_Ne20s, delta\_Ne40s) indicates the electron density fluctuations smaller than 75 km (150 km, 300 km) for Swarm.

Grad\_Ne@100km (Grad\_Ne@50km, Grad\_Ne@20km) is the electron density gradient ( $\nabla Ne$ ) in a running window of 27 (13, 5) data points, which corresponds to a spatial scale of 100 km (50 km, 20 km) for Swarm. The electron density gradient is calculated using a linear regression over a certain time interval. An example of the density gradient is shown in Figure 4.2.1. The top panel shows the original electron density (2 Hz) in blue, and the linear fits of the intervals centred at 18:21.40 universal time (UT) are shown in green, black and red dashed lines. The bottom panel shows the density gradients calculated in respective running windows.

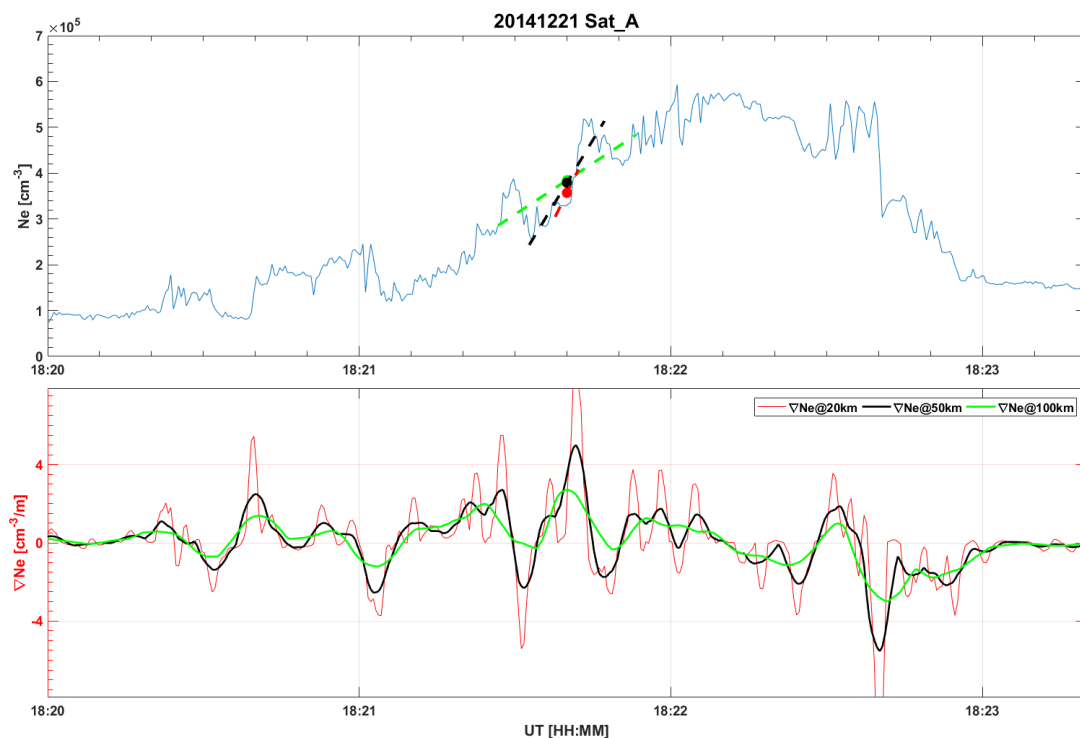


Figure 4.2.1. (top) The electron density and linear fits determining density gradients centred at 18:21.40 UT using three different windows (scales). (bottom) Density gradients calculated in respective running windows corresponding to different scales. Example data are from Swarm A, 21 Dec. 2014.

The background density ( $bNe$ ), foreground density ( $fNe$ ), polar cap patch index, and electron density gradient near the edge of a polar cap patch ( $Grad\_Ne@PCP\_edge$ ) are taken from the Polar Cap Products (PCP) (Spicher et al., 2017). The background density is calculated from  $Ne$  using a 35<sup>th</sup> percentile filter of 551 data points (~2000 km for 2 Hz data and the Swarm speed of ~7.5 km/s). The foreground density is calculated from  $Ne$  using a 50<sup>th</sup> percentile filter of 7 data points (~25 km). The polar cap patch index is an indication of whether the measurement is taken within a polar cap patch, see Table 1 for more details.  $Grad\_Ne@PCP\_edge$  is the linear electron density gradient calculated over the edge of a polar cap patch and it is non-zero only on the edges of polar cap patches.

Finally, to provide the compatibility with the GPS and magnetic field datasets, we down-sample the plasma density (and parameters derived from  $Ne$ ) and the electron temperature data to 1Hz. Figure 4.2.2 shows an example of the down-sampled data in red, while the raw 2 Hz data in blue. One example of the final data is shown in Figure 4.2.3. The down-sampling of derived parameters assures that they are being calculated using the 2Hz resolution data and give a more accurate description of the plasma density variations.

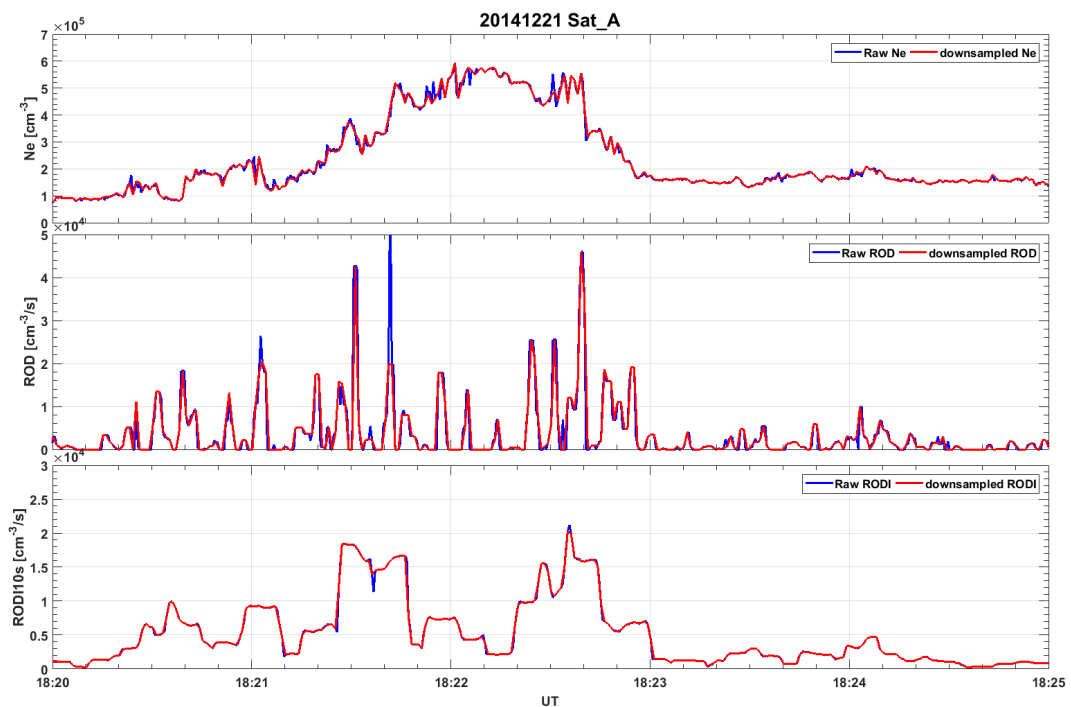


Figure 4.2.2. Example of the high resolution (raw) data in blue color, and the down-sampled data in red color from Swarm A. Note that ROD is rectified to show only the absolute value.

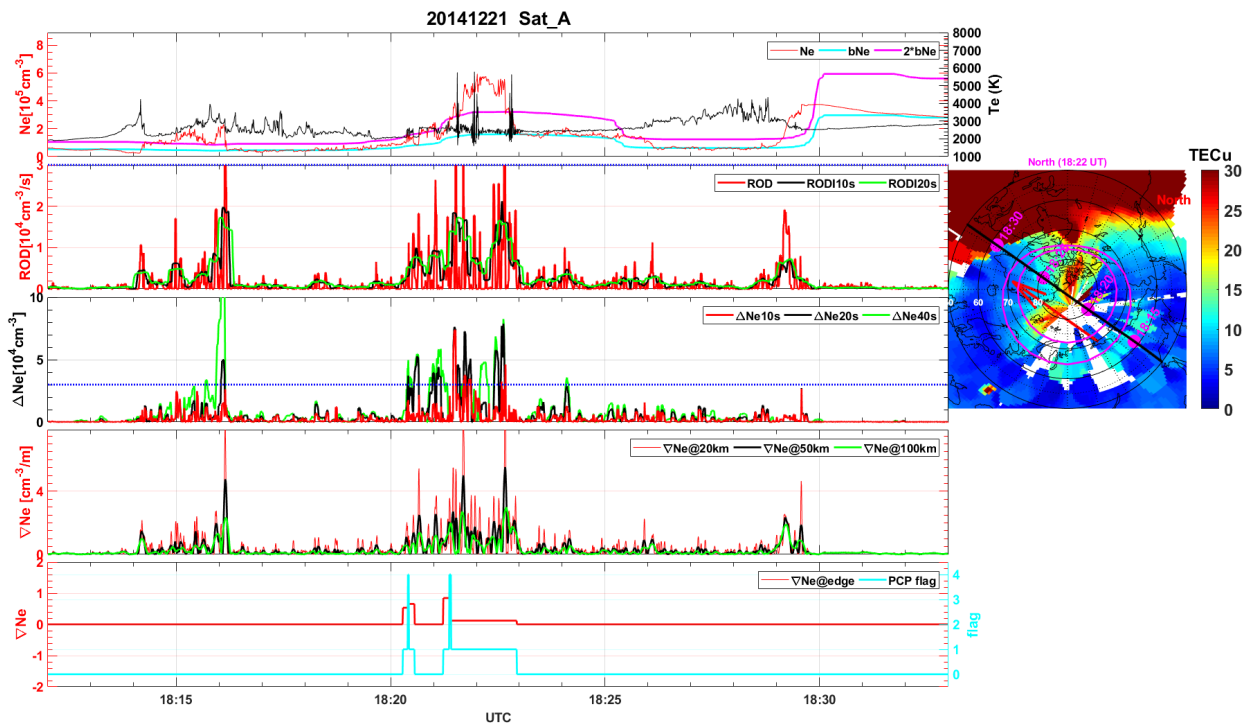


Figure 4.2.3. Example of parameters derived from the electron density data from Swarm A. Note that ROT,  $\Delta Ne$  and  $\nabla Ne$  are rectified to show the absolute values. Map to the right shows the global GPS TEC map. The Swarm orbit is presented as black line with the timestamps annotated in magenta.

### 4.2.3 ROT and ROTI from the GPS TEC data

The GPS TEC data are taken from the Swarm L2 TEC product (TECxTMS\_2F). We derive parameters characterizing the fluctuations of TEC along the ray paths from the Swarm satellites to GPS satellites. Those parameters include Rate of change of TEC (ROT), Rate of change of TEC index (ROTI).

ROT is the time derivative of TEC define as follows:

$$ROT(t) = \frac{TEC(t + \Delta t) - TEC(t)}{\Delta t}$$

And here  $\Delta t = 1 \text{ second}$ , since we use the 1 Hz GPS TEC data.

ROTI10s (ROTI20s) is the standard deviation of ROT in a running window of 10 (20) seconds:

$$ROTI(t) = \sqrt{\frac{1}{N-1} \sum_{t_i=t-\Delta t/2}^{t_i=t+\Delta t/2} |ROT(t_i) - \overline{ROT}|^2}$$

and  $\overline{ROT}$  is the mean of  $ROT(t_i)$ :

$$\overline{ROT} = \frac{1}{N} \sqrt{\sum_{t_i=t-\Delta t/2}^{t_i=t+\Delta t/2} ROT(t_i)}$$

where  $\Delta t = 10$  or  $20 \text{ seconds}$ .

For calculating ROT and ROTI, only the GPS satellites with elevation angles larger than 30 degrees are used. This is to avoid signals traveling through high density ionosphere at low elevation angles far from the Swarm satellite, and ensure that the local plasma conditions are studied.

### 4.3 Assigning plasma irregularities to geomagnetic regions

In the IPIR product, the following geomagnetic regions with respect to latitude have been specified:

- Equatorial region
- Mid-latitudes
- Auroral oval
- Polar Cap

These regions reflect different ionospheric plasma conditions and allow the user to perform large statistical studies and relating ionospheric irregularities to different processes. Equatorial region is defined between  $\pm 30^\circ$  MLAT, according to several previous studies (e.g., Park et al. 2010) and in accordance to the IBI L2 product. Mid-latitudes is a region between  $\pm 30$  MLAT and the equatorward Auroral Oval Boundary (AOB). The extent of the Auroral oval is dynamic, and AOBs depend on geomagnetic activity. Thus, AOBs are defined with the use of the Field-Aligned Current (FAC) method, as described in the next subsection. The polar cap is defined as poleward of the auroral oval, or when the poleward boundary of the oval is not found, it is poleward of  $77^\circ$  MLAT, as defined in the PCP product.

#### 4.3.1 Auroral oval boundaries: the FAC method

The best-known auroral features are the Northern and Southern auroral ovals (Feldstein et al., 1969) that are the regions in the ionosphere receiving the main part of the magnetospheric particle precipitation. The dynamics of the auroral oval is related to geomagnetic activity, and the exact locations of the boundaries depend on the energy of precipitating particles as well as the magnetospheric electric and magnetic fields (Kauristie et al., 1999). The boundaries of the auroral oval can be determined locally by ground-based observations such as radars (Pinnock and Rodger, 2000; Moen et al., 2004) or low-altitude satellite observations (Wang et al., 2005). Auroral boundaries can be detected from small-scale FAC signatures in the magnetic field as observed by satellites (Newell et al. 1989, Lorentzen 2000, Xiong et al. 2014). Thus, Swarm satellites, with high-resolution magnetometers on-board provide precise global coverage of the auroral boundaries.

Estimates of FACs (single satellite method) are routinely derived from the magnetic measurements of each Swarm spacecraft and provided as the L2 data product FACxTMS\_2F. For determining the auroral boundaries, we use the small-scale (up to 10 km) FAC part of this data product. Larger scales are suppressed by subtracting 20 s averaged values, corresponding approximately to 150 km along Swarm orbits, as the auroral boundaries are more sharply detected from the small-scale FACs.

Figure 4.3.1 (a) presents an example of the small-scale FACs activity (top panel) at auroral latitudes on 27 January 2015 derived from Swarm A. There is a well-defined latitude range, marked by high FAC intensity that can be associated with the auroral oval. The magnetic quasi-dipole (QD) latitude (Richmond, 1995) used here facilitates a mapping of FACs at satellite height along geomagnetic field lines down to the ionospheric E-layer (about 110 km altitude). Further, a variable  $S$  has been used to represent the FAC intensity, which is defined as  $S = \langle \log_{10} j_{\parallel}^2 \rangle_{20s}$ .

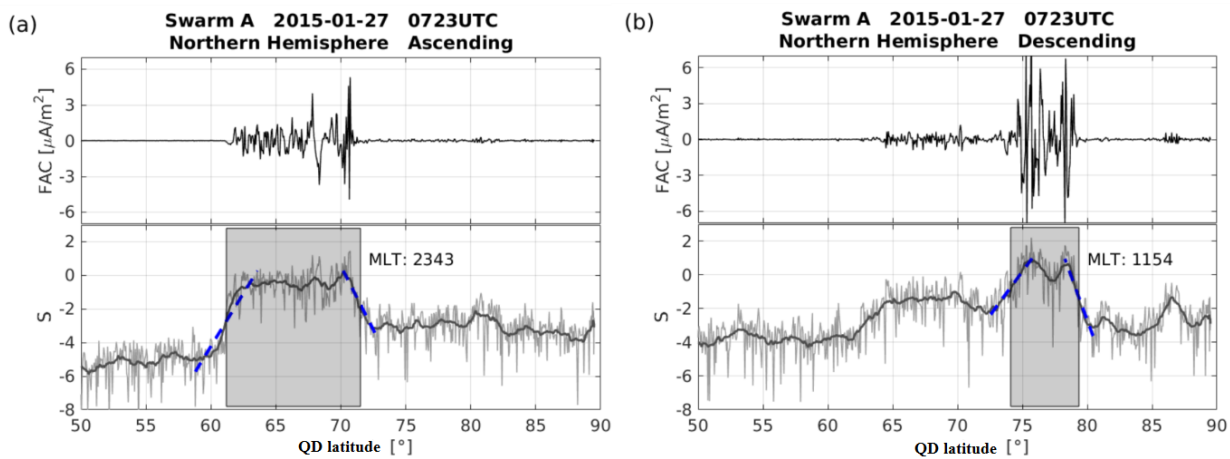


**Figure 4.3.1** Two examples of auroral boundaries derived from high-latitude FAC measurements of Swarm A around 0723 UTC on 27 January 2015 for (a) ascending and (b) descending arcs. In each example, the top panels present the small-scale FACs and the bottom panels show the corresponding  $S$  curves for detecting auroral boundaries. In the bottom panel, the grey thin line indicates the variations of  $S$  value, and the grey thick line is the 20 s averaged value of  $S$ . The blue dashed line is the linear part of  $S$  value with steep gradients, representing the equatorial and poleward boundaries, respectively, and the grey shadow area indicates the auroral oval derived by our approach.

Because of a wide range of variations encountered during a boundary crossing, we consider the logarithm of the squared current density (to avoid negative values in in logarithm). The FAC density,  $j_{\parallel}$ , is given in units of  $\mu\text{A}\cdot\text{m}^{-2}$ . We take averages over 20 s for the values of  $S$ . The latitude profiles of FACs and corresponding  $S$  values are then calculated individually along the four high-latitude segments (from  $\pm 50^\circ$  QD latitude to the magnetic pole in both hemispheres) for each Swarm orbit. Data from these segments were surveyed subsequently by an automatic procedure to find the linear parts of the  $S$  curve with steep gradients. We start to check from the latitude of maximum  $S$  value to lower and higher latitudes for equatorward and poleward boundaries, respectively.

The bottom panel of Figure 4.3.1 (a) illustrates the detection procedure described above. The blue dashed lines indicate the linear part with steep gradients of  $S$  value at both equatorward and poleward, and the shadowed area indicates the derived auroral oval. Similarly, Figure 4.3.1 (b) presents the consecutive arc (descending node) of small-scale FACs observed by Swarm A.

The processing flow of the FAC algorithm for Swarm AOB consists of five main modules:

- Module 1: (Sect. 4.3.1.1)
- Module 2: data pre-processing (Sect. 4.3.1.2)
- Module 3: finding the auroral equatorial boundary (Sect. 4.3.1.3)
- Module 4: finding the auroral poleward boundary (Sect. 4.3.1.4)
- Module 5: saving of Swarm AOB data (Sect. 4.3.1.5)

#### 4.3.1.1 *Module 1: read configuration file*

The following list describes the single processing steps in the module 1:

- Read configuration file for the given Swarm satellite
- Create and return an internal data structure as input for the other modules: **data-m1**



#### 4.3.1.2 *Module 2: data pre-processing*

The following list describes the single processing steps in the module 2:

- Take over: **data-m1** (Sect. 4.3.1.1)
- Read input:
  - a. FAC data of the previous day
  - b. FAC data of the current day
- Combine the FAC data of the previous and current day
- Calculate the Magnetic Local Time (MLT) and Magnetic Latitude (MLat), i.e. QD latitude
- Divide the data into orbits and find out the high-latitude orbital arcs:  $|\text{MLat}| > 50^\circ$
- For each high-latitude orbital arc, the FAC data are first filtered, to suppress the larger-scales FAC by subtracting 20 s averaged values
- The rest of small-scale FAC are converted to  $S$  value, which represents the intensity of FAC, averages over 20 s are taken for the values of  $S$ .
- Return all input variables, magnetic coordinates, and values of  $S$  as internal data structure: **data-m2**

#### 4.3.1.3 *Module 3: finding the auroral equatorial boundary*

The following list describes the single processing steps in the module 3:

- Take over: **data-m2** (Sect. 4.3.1.2)
- Find the maximum  $S$  value of the considered orbital arc
- From the maximum value towards equatorward, find the linear part of  $S$  value with deepest slope
- The middle points of the linear part is then taken as the auroral equatorial boundary
- If no linear part of the  $S$  value is identified, the auroral equatorial boundary is recorded as *NaN* value
- Return time, location, and magnetic coordinates: **data-m3**

#### 4.3.1.4 *Module 4: finding the auroral poleward boundary*

The following list describes the single processing steps in the module 4:

- Take over: **data-m2** (Sect. 4.3.1.2)
- From the maximum value towards poleward, find the linear part of  $S$  value with deepest slope
- The middle points of the linear part is then taken as the auroral poleward boundary
- If no linear part of the  $S$  value is identified, the auroral poleward boundary is recorded as *NaN* value
- Return time, location, and magnetic coordinates: **data-m4**

#### 4.3.1.5 *Module 5: saving of Swarm AOB data*

The following list describes the single processing steps in the module 5:

- Take over: **data-m3** (Sect. 4.3.1.3)
- Take over: **data-m4** (Sect. 4.3.1.4)
- Save AOB data to CDF file. Details on the specification and content of the CDF file are found [AD-4].

## 4.4 Determining the IPIR-index

Based on the characteristics of ionospheric irregularities, the IPIR index  $\zeta$  is evaluated. The IPIR index is calculated as a product of RODI10s and  $\text{delta\_Ne\_windowed}$ , which is a moving standard deviation of  $\text{delta\_Ne10s}$  chosen in a running window of 10 seconds for consistency with RODI10s. Since RODI is the variance of fluctuations in density and it indicates structuring of the plasma within the 10 seconds interval. On the other hand,  $\text{delta\_Ne\_windowed}$ ,  $A(\text{Ne})$ , provides the absolute amplitude of fluctuations in plasma over a given time interval. Thus, combining these two parameters describes the severity of irregularities, where high frequency fluctuations with large amplitudes are the most severe. Such irregularities can have the largest space weather impacts such as affecting trans-ionospheric radio signals. Note, that these two parameters

are only weakly correlated, thus their combination is statistically sound. The IPIR index  $\zeta$  is determined as following:

$$\zeta = RODI10s \cdot A(Ne)_{10s},$$

where  $A(Ne)_{10s}$  is the standard deviation of  $\Delta Ne10s$  in a running window of 10 seconds:

$$A(Ne)_{10s}(t) = \sqrt{\frac{1}{N-1} \sum_{t_i=t-\Delta t/2}^{t_i=t+\Delta t/2} |\Delta Ne10s(t_i) - \overline{\Delta Ne10s}|^2}$$

where  $\overline{\Delta Ne10s}$  is the mean of  $\Delta Ne10s(t_i)$ :

$$\overline{\Delta Ne10s} = \frac{1}{N} \sum_{t_i=t-\Delta t/2}^{t_i=t+\Delta t/2} \Delta Ne10s(t_i)$$

The scale of the IPIR index has been determined by comparison with the ground-based observations of the ionospheric scintillations. The scale ranges from 1 to 8 and it corresponds to the logarithmic scale of  $\zeta$  numerical values:

IPIR index scale	Numerical value of $\zeta$ [ $\text{cm}^{-3}\text{s}^{-1}\text{cm}^{-3}$ ]	Likelihood of phase scintillations
1	$< 10^3$	Insignificant
2	$10^3\text{-}10^4$	Low
3	$10^4\text{-}10^5$	Low
4	$10^5\text{-}10^6$	Medium
5	$10^6\text{-}10^7$	Medium
6	$10^7\text{-}10^8$	High
7	$10^8\text{-}10^9$	High
8	$> 10^9$	Very high

## 5 Description of the output data

One data file for each Swarm-IPIR product is produced per day and per Swarm satellite (Alpha, Bravo, or Charlie). A daily CDF file is generated only when the corresponding Level 1b (L1b), L2, and/or model files for the given satellite and date are available. Detailed description of the output variables including type, description, and units can be found in [AD-4].

## 6 Selected Examples

In this section, selected examples from the IPIR product are shown. Figure 6.1 shows results for one full orbit from South to North for Swarm A on 08 September 2017. This corresponds to a local time in the morning hours (10 LT). Equatorial ionosphere is very smooth (17:45-17:55 UT), while the high latitude ionosphere shows large irregularities visible both in ROD, RODI, ROT, and ROTI. The field aligned currents (FAC) are well detected. Small inset to the right shows the trajectory of the satellite over a contour map with background TEC values representing the background density (taken from the ground-based measurements).

Figure 6.2 shows another example of data taken for the evening local time on the same day, this time at pre-midnight. As expected, the equatorial ionosphere is subject to bubbles (localised density depletions), and it is characterised by large irregularities. Irregularities in the high-latitude ionosphere are due to polar cap patches and auroral blobs.

Finally, in Figure 6.3, we show an example of main IPIR parameters during one flight over the north polar region, as indicated in the inset-map to the right. The irregular structures can be associated with localised enhancements in the plasma density - polar cap patches.

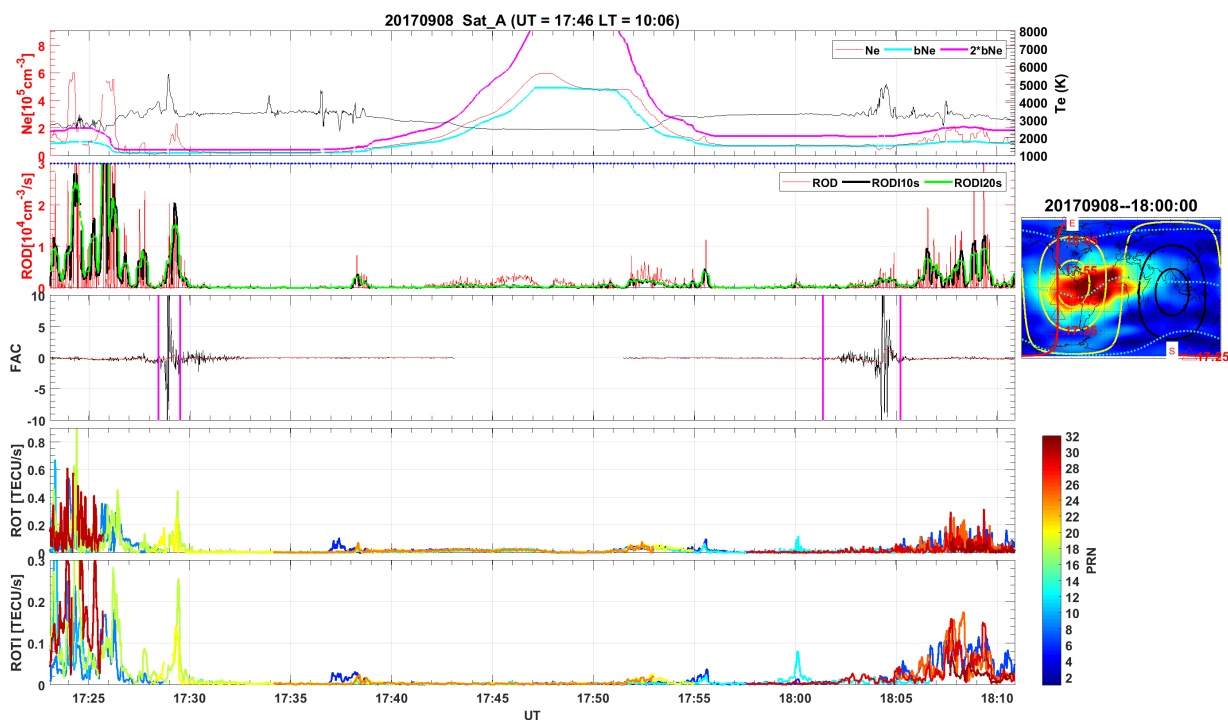


Figure 6.1. Example of the parameters during one full orbit from the South to the North for Swarm A, for 08 September 2017 around 10 hours local time (LT). Note that ROD and ROT are rectified to show the absolute values.

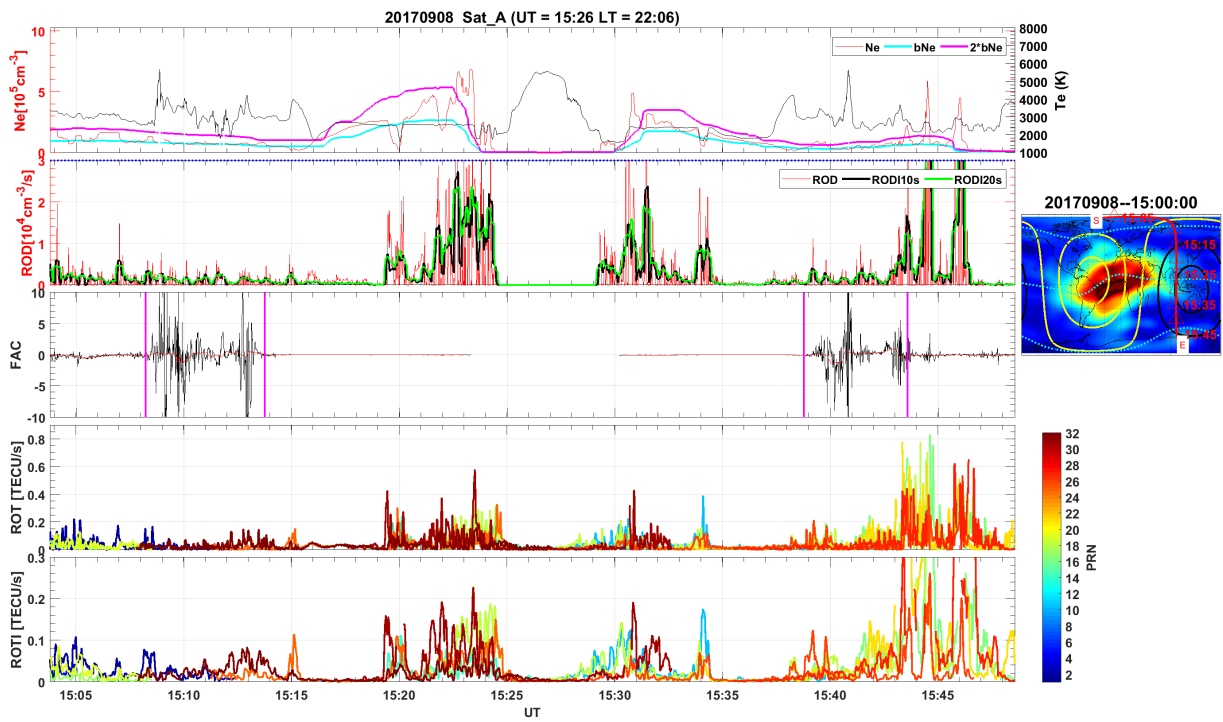


Figure 6.1. Example of the parameters during one full orbit from the North to the South for Swarm A, for 08 September 2017 around 22 hours LT. Note that ROD and ROT are rectified to show the absolute values.

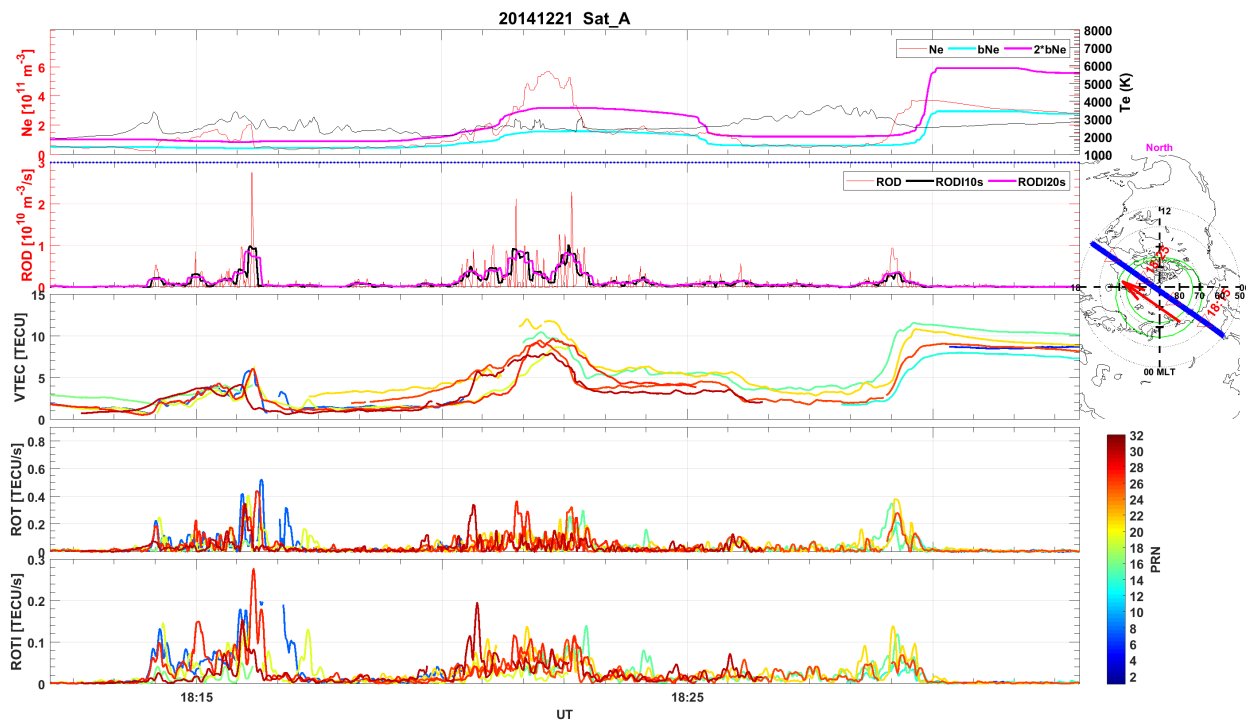


Figure 6.3. An example of IPIR parameters during one of the Swarm A flights over the north polar region on 21 December 2014. Note that ROD and ROT are rectified to show the absolute values.